Journal of Solid State Chemistry **154,** 427–434 (2000)
doi:10.1006/jssc.2000.8860, available online at http://www.idealibrary.com on IDEAL®

An X-Ray Powder and Electron Diffraction Study of Reduced Tantalates with the Perovskite Structure, $Na_{1-x}Sr_xTaO_3$, $0 < x \leq 0.4$

S. Ya. Istomin,*,[1] G. Svensson,†,[2] H. Hannerz,† and J. Köhler*

*Max-Planck-Institut für Festkörperforschung, D-70569 Stuttgart, Germany; and †Department of Structural Chemistry, Stockholm University, 10691 Stockholm, Sweden

Received January 31, 2000; in revised form June 14, 2000; accepted July 13, 2000; published online September 30, 2000

Single-phase perovskite-type reduced tantalates, $Na_{1-x}Sr_xTaO_3$ with $0 < x \leq 0.4$, have been synthesized by heating mixtures of $NaTaO_3$, $Sr_5Ta_4O_{15}$ and Ta in sealed tantalum ampules at 1400°C for 20–24 h. At Sr contents of $0.5 \leq x \leq 0.8$ and above 1400°C, polyphasic samples were obtained. X-ray powder diffraction (XRD) and transmission electron microscopy studies (selected area (SAED) and convergent beam electron diffraction (CBED)) showed an orthorhombic distortion of the $x = 0.1$ sample ($GdFeO_3$ type, space group *Pnma*). The interpretation of the XRD, SAED, and CBED studies indicates the crystallites found in the $x = 0.2$ and 0.3 samples to consist of domains with tetragonal and orthorhombic symmetry having the unit cell parameters of $a = b \approx \sqrt{2}a_{per}$ and $c \approx 2a_{per}$ and $a \approx b \approx \sqrt{2}a_{per}$ and $c \approx a_{per}$ (a_{per} cell axis in the ideal perovskite structure), respectively. The $x = 0.4$ sample was cubic (space group *Pm3m*) with $a = a_{per}$. Resistivity measurements showed that all samples are semiconducting and that the conductivity increases with Sr content. Magnetic measurements of $Na_{0.6}Sr_{0.4}TaO_3$ revealed a diamagnetic behavior down to 20 K. Below this temperature a slight paramagnetism arises. © 2000 Academic Press

Key Words: **reduced oxotantalate; perovskite; electron diffraction; crystal structure; X-ray powder diffraction.**

INTRODUCTION

It is well known that the stability of mixed-valence early transition metals decreases down the groups and is reflected in the chemistry of vanadium, niobium, and tantalum. There are numerous reduced oxovanadates reported in the literature. Oxoniobates are more reluctant to be reduced, and often hydrogen, carbon, or niobium is needed as a reducing agent. Complex oxides containing niobium with a d^0 to d^1 electron configuration often have perovskite-based structures, as in Sr_xNbO_3 (perovskite) (1, 2) and $Ba_6Nb_{10}O_{30}$ (tetragonal tungsten bronze (TTB) type) (3), respectively.

Such slightly reduced oxoniobates have attracted some interest in recent years as promising candidates for new non-copper-based superconductors. Only a few perovskite-related compounds are reported to be superconducting in these systems, e.g., Li-intercalated $KCa_2Nb_3O_{10}$ (4). In more reduced oxoniobates with an electron configuration close to d^2, niobium–niobium bonded units are frequently found, such as the Nb_6O_{12} clusters (5). Tantalum is even more averse than niobium to adopt an oxidation state lower than maximal, and very few reduced complex tantalum oxides are reported in the literature. Tantalum with an electron configuration between d^0 and d^1 is found in $Sr(Ba)_6Ta_{10}O_{30}$ (6, 7), (TTB) and $Ca_2Ta_2O_6F$ (6) with the pyrochlore-type structure. Recently, there have been also reports of reduced compounds with a layered perovskite-type structure, as in $Li_2LaTa_2O_7$ (8), as well as more reduced oxotantalates containing metal clusters: $Mn_{0.58}Ta_3O_6$ (9) and $MAl_2Ta_{35}O_{70}$ (M = Na, K, Rb) (10), and also $Ba_2Ta_{15}O_{32}$. (7).

We have been investigating oxoniobates with various degrees of reduction for several years. In the present report we have turned our interest to reduced oxotantalates with the perovskite-type structure. There are several perovskite-type Ta^{5+} oxocompounds, such as $NaTaO_3$ and $KTaO_3$, but no reduced analogues have been reported. The room-temperature modification of $NaTaO_3$ has the orthorhombic $GdFeO_3$-type structure; the compound is an electric insulator. One way of increasing the conductivity of $NaTaO_3$ perovskite is to replace Na^+ with Sr^{2+}. This substitution will introduce charge carriers in the t_{2g}-like band of the octahedrally coordinated Ta atoms and thereby increase the conductivity (11). It has been shown that these electrons will enter M–O π-bonding orbitals and will favor an M–O–M bond angle of 180° (12, 13). As a consequence and neglecting

[1] Permanent address: Department of Chemistry, Moscow State University, 119899 Moscow, Russia.

[2] To whom correspondence should be adressed. Tel.: + 46 8 16 12 54. Fax: + 46 8 16 31 18. E-mail: gunnar@struc.su.se.

0022-4596/00 $35.00
Copyright © 2000 by Academic Press
All rights of reproduction in any form reserved.

the geometrical factor, one may expect the symmetry of $NaTaO_3$ to change from orthorhombic toward cubic when Na is replaced with Sr.

In this paper we report on the novel preparation, crystal structure, and electric and magnetic properties of the reduced tantalates $Na_{1-x}Sr_xTaO_3$, $0 < x \leq 0.4$, with the perovskite structure

EXPERIMENTAL

Samples of $Na_{1-x}Sr_xTaO_3$, $0 < x \leq 0.8$, were prepared by annealing pellets of stoichiometric mixtures of $NaTaO_3$, $Sr_5Ta_4O_{15}$, and Ta (99.99%) in tantalum tubes, sealed by welding under Ar, at 1400–1600°C for 20–24 h. $NaTaO_3$ and $Sr_5Ta_4O_{15}$ were prepared by heating stoichiometric amounts of Na_2CO_3 or $SrCO_3$ and Ta_2O_5 first at 800°C for 48 h and then at 1200°C for another 48 h in air.

X-ray powder diffraction (XRD) data for the Rietveld refinements were collected on a STOE STADI-P powder diffractometer equipped with a mini-PSD detector, with a rotating sample in symmetric transmission mode (germanium monochromator, Cu$K\alpha_1$ radiation). The RIETAN 97 program package was used for the refinement (14).

For the transmission electron microscopy (TEM) studies small amounts of the samples were crushed in *n*-butanol. A drop of this dispersion was put on a holey carbon film supported by a copper grid. Electron diffraction (ED) studies were carried out with a JEOL JEM 2000 FX instrument operated at 200 kV. For the determination of the cation content, microanalyses of the individual crystallites on the same grids as studied in the TEM were performed with in a JEOL JSM 880 scanning electron microscope equipped with a windowless energy-dispersive analyzer (EDS), LINK Isis. Simulated electron diffraction patterns were prepared with the program suite MacTempas (15).

Atomic emission spectroscopy with inductively coupled plasma (analyzer ARL 3580B ICP) was used for the chemical analysis. For the ICP analysis the samples were dissolved in a mixture of HNO_3 and HF (2:0.25) in a nickel bomb for 20 h.

The temperature dependence of the resistance of the samples of $Na_{1-x}Sr_xTaO_3$, $x = 0.1, 0.2, 0.3, 0.4$, was measured on pellets of approximately $3 \times 4 \times 4$ mm in size by a normal four-probe method in the temperature range 2–300 K. The magnetic susceptibility of the $x = 0.4$ sample was measured in the temperature range 2–300 K.

RESULTS AND DISCUSSION

Black monophasic samples of the perovskite-type compounds $Na_{1-x}Sr_xTaO_3$ were obtained for $0 < x \leq 0.4$ at $T = 1400$°C. The samples with $x \geq 0.5$ were polyphasic and contained, together with the perovskite phase $Na_{1-x}Sr_xTaO_3$, unreacted $Sr_5Ta_4O_{15}$, and Ta(m). Increasing the annealing temperature above 1400°C did not increase the homogeneity region of $Na_{1-x}Sr_xTaO_3$. Reannealing as well as increased heating time led to sodium losses and eventually to the formation of phases with TTB-type structure. For example, a sample with $x = 0.5$ annealed at 1600°C for 48 h consisted of a single-phase TTB-type compound with the unit cell parameters $a = 12.3797(3)$ and $c = 3.8695(1)$ Å. Determination of the cation content of this phase suggested the composition $Na_{0.90}Sr_{4.70}Ta_{10}O_{30}$ (normalized to 10 tantalum atoms). Small but significant sodium losses during annealing were also found for the samples heated at 1400°C, as shown in Table 1. These results show that the $A = Na + Sr$ position is not always fully occupied in these perovskite-type oxotantalates. An attempt to synthesize the tantalum analogues of the known perovskite-type strontium oxoniobates $Sr_{0.8}NbO_3$ and

TABLE 1
Composition and Crystal Data for $Na_{1-x}Sr_xTaO_3$, $0 = x \leq 0.4$

Phase	$Na_{0.6}Sr_{0.4}TaO_3$	$Na_{0.7}Sr_{0.3}TaO_3$	$Na_{0.8}Sr_{0.2}TaO_3$	$Na_{0.9}Sr_{0.1}TaO_3$	$NaTaO_3$ (18)
Composition[a]	$Na_{0.5}Sr_{0.4}TaO_3$	$Na_{0.6}Sr_{0.3}TaO_3$	$Na_{0.8}Sr_{0.2}TaO_3$	$Na_{0.8}Sr_{0.1}TaO_3$	—
Space group	*Pm3m*	*P4/mmm*	*P4/mbm*	*Pnma*	*Pnma*
Unit cell parameters,[b] Å		$a = 3.94756(5)$	$a = 5.55532(4)$	$a = 5.51290(8)$	$a = 5.5213(2)$
	$a = 3.96291(3)$	$c = 3.93993(7)$	$c = 3.94625(3)$	$b = 7.8328(1)$	$b = 7.7952(2)$
				$c = 5.53619(8)$	$c = 5.4842(8)$
Cell vol. (sub cell), Å^3	62.24	61.40	121.79 (60.9)	239.06 (59.8)	236.04 (59.0)
Z	1	1	2	4	4
2θ range	$15 < 2\theta < 130$	$7 < 2\theta < 100$	$10 < 2\theta < 130$	$10 < 2\theta < 120$	
Step length, 2θ	0.02	0.02	0.02	0.02	
R_I, R_P[c]	0.034, 0.046	0.026, 0.047	0.025, 0.039	0.028, 0.049	

[a] According to chemical analysis data.
[b] From Rietveld refinement.
[c] R_P was calculated taking into account Si used as internal standard. R_I calculated for Si does not exceed 0.04 in any of the diffraction experiments.

$Sr_{0.7}NbO_3$, at 1650°C for 24 h, resulted in mixtures of $Sr_2Ta_2O_7$ (16) and $Sr_6Ta_{10}O_{30}$ (6, 7).

X-Ray Study

The unit cell parameters for the $Na_{1-x}Sr_xTaO_3$ phase, $0 \leq x \leq 0.4$, are given in Table 1. Two main features can be observed: the size of the perovskite subcell increases with increasing strontium content, and the symmetry of the lattice changes in the sequence orthorhombic–tetragonal–cubic.

For $x = 0.1$, a distinct splitting of the perovskite subcell reflections (*hhh*) and (*h*00) was observed in the XRD pattern, indicating a monoclinic structure, see Fig. 1a. However, the presence of superstructure reflections suggested an orthorhombic unit cell $a \approx \sqrt{2}a_{per}$, $b \approx 2a_{per}$, $c \approx \sqrt{2}a_{per}$ (space group *Pnma*, a_{per} cell axis in the ideal perovskite structure). It should be mentioned that only one reflection corresponding to $b \approx 2a_{per}$ was found, as shown in Fig. 1. It is a result of overlap between the (211), (112), and (031) reflections, each having a relative calculated intensity of about $I_{rel} = 0.4\%$. All other superstructure reflections have much lower intensity.

For $x = 0.2$, a clear split of the perovskite subcell reflections (except (*hhh*)) and weak superstructure reflections ($I_{rel} \approx 1\%$) suggesting a tetragonal unit cell were observed in the XRD, as shown in Fig. 2. They can only be indexed on the basis of a doubled perovskite cell, with one even and two odd indices. This corresponds to the one-tilt system of the type $a^\circ a^\circ c^+$ (No. 21) according to Glazer (17). The appropriate unit cell is then $a = b \approx \sqrt{2}a_{per}$, $c \approx a_{per}$ and the space group is *P*4/*mbm*. This superstructure type is also found for $NaTaO_3$ at $T = 893$ K (18).

For $x = 0.3$ no superstructure reflections were found in the X-ray patterns, although a splitting of the reflections was observed as a nonmonotonic increase of full width at half-maximum (FWHM) versus 2θ, as shown in Fig. 3, indicating a tetragonal unit cell. The effect is especially clear for the 200, 310, and 311 reflections. The XRD pattern of $Na_{0.7}Sr_{0.3}TaO_3$ was consequently indexed with a tetragonal cell: $a \approx a_{per}$, $c \approx a_{per}$.

For $x = 0.4$, the increase of FWHM of the XRD reflections with increasing Bragg angle is shown in Fig. 4. The monotonic increase, together with the absence of superstructure reflections in the XRD patterns, suggests the compound to have an ideal perovskite structure with $a = a_{per}$ and space group *Pm*3*m*.

The crystal structures of $Na_{1-x}Sr_xTaO_3$, $0 < x \leq 0.4$, were refined using the XRD data. The cationic occupancies were fixed according to the results from the chemical analyses. Isotropic thermal factors were used for all atoms and a collective one was used for the oxygen atoms. During the refinement of $Na_{0.9}Sr_{0.1}TaO_3$ a negative thermal parameter was obtained for oxygen, and it was consequently fixed at 1.5 in the final refinements. Final *R*-factors, atomic coordinates, and selected interatomic distances and angles for $Na_{1-x}Sr_xTaO_3$, $0 < x \leq 0.4$, are given in Tables 1, 2, and 3, respectively. The results from the refinement of the $x = 0.2$ and 0.3 samples only provide information on an average structure because the ED studies, to be discussed below, showed the true unit cells to be larger than those found from the XRD data.

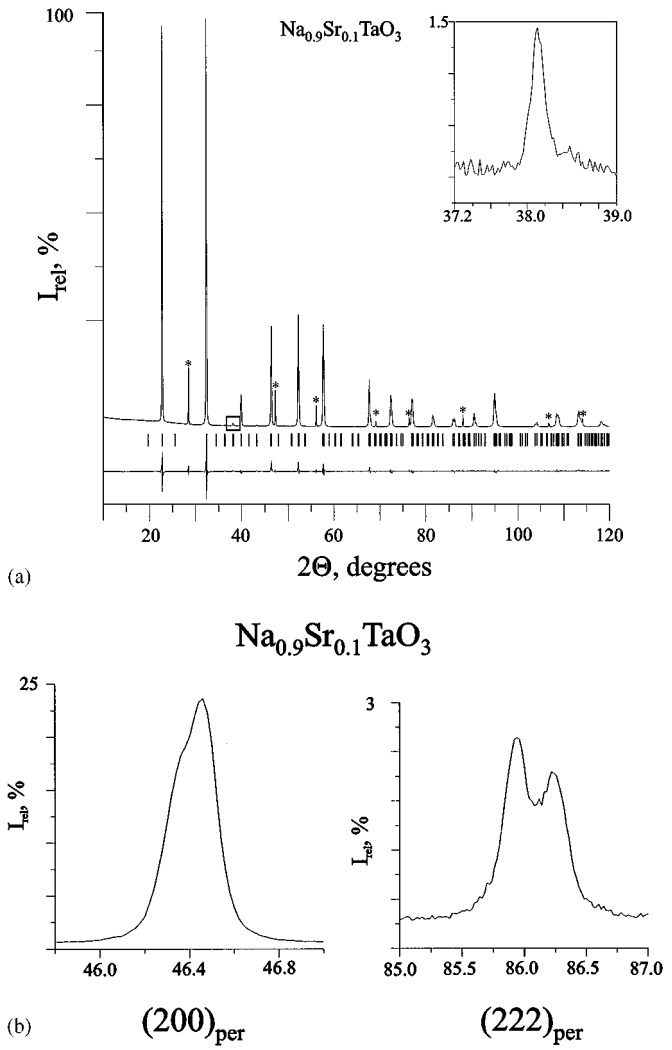

FIG. 1. (a) XRD pattern of a sample with nominal composition $Na_{0.9}Sr_{0.1}TaO_3$, with an enlargement showing the reflection that corresponds to the $b = 2a_{per}$ axis. It is an overlap between 211, 112, and 031 reflections and confirms the unit cell to be $a \approx \sqrt{2}a_{per}$, $b \approx 2a_{per}$, $c \approx \sqrt{2}a_{per}$. (b) Magnification of the split $(222)_{per}$ and $(200)_{per}$ XRD peaks, indicating an orthorhombic structure.

Electron Diffraction Study

The perovskite-type structure is often slightly distorted, which is important in determining the properties of the

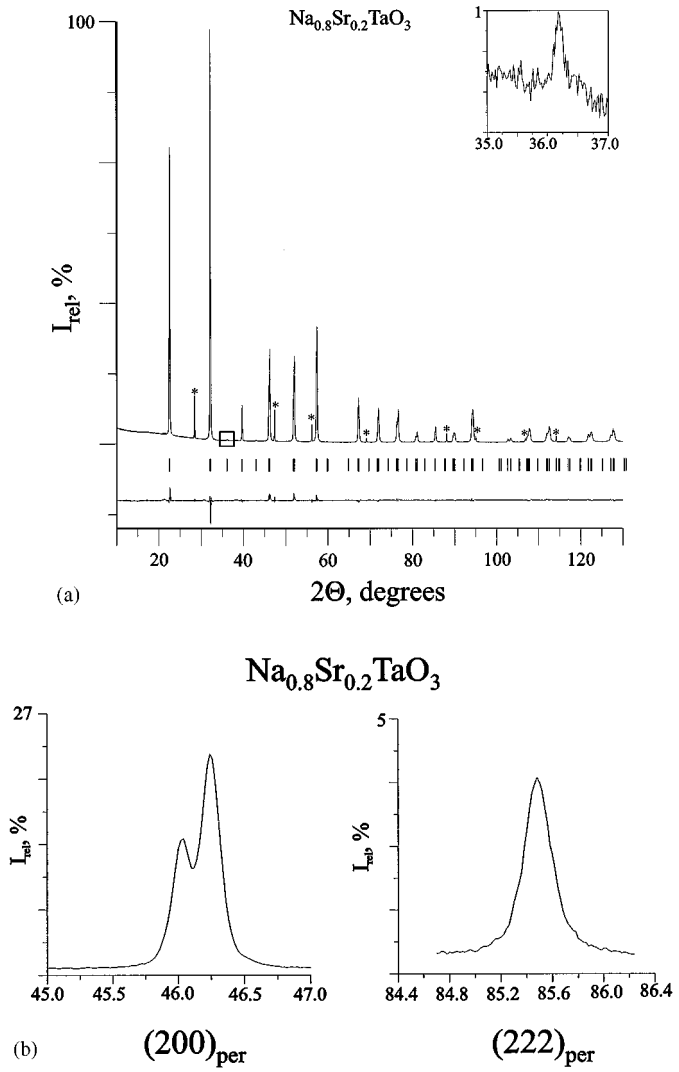

FIG. 2. (a) XRD pattern of a sample with nominal composition $Na_{0.8}Sr_{0.2}TaO_3$, with one weak superstructure reflection magnified. This reflection indicates the appropriate unit cell to be $a = b \approx \sqrt{2}a_{per}$, $c \approx a_{per}$. (b) Magnification of the unsplit $(222)_{per}$ and the split $(200)_{per}$ XRD peaks, suggesting tetragonal symmetry.

compound. However, the superstructure reflections resulting from small distortions are often so weak that they cannot be detected in normal XRD investigations. In contrast, even weak superstructure reflections are often clearly seen in selected-area electron diffraction patterns (SAED), and the symmetry can be determined by convergent-beam electron diffraction (CBED) techniques. We therefore made an electron diffraction study of the $x = 0.1$, 0.2, 0.3, and 0.4 samples to investigate the presence of superstructure reflections and to confirm the tetragonal symmetry of the $x = 0.2$ and 0.3 samples.

For $x = 0.1$, the SAED study confirmed the space group *Pnma* and the unit cell parameters $a \approx \sqrt{2}a_{per}$, $b \approx 2a_{per}$, and $c \approx \sqrt{2}a_{per}$ found in the XRD study discussed above.

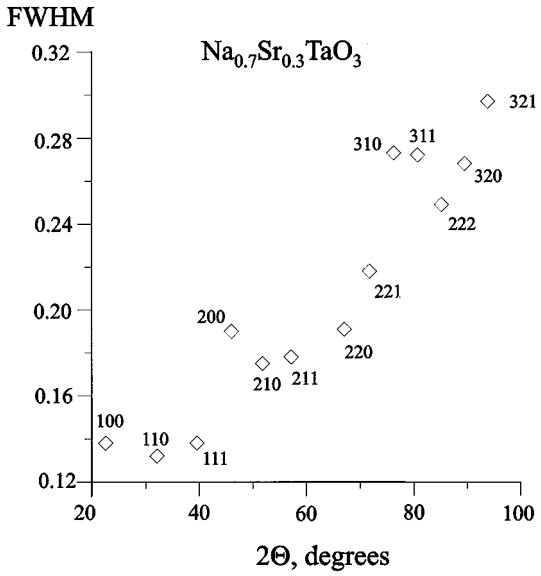

FIG. 3. Tetragonal symmetry is indicated by the nonmonotonic increase with increasing Bragg angle, 2θ, of the full width at half-maximum of the XRD reflections from the sample with the nominal composition $Na_{0.7}Sr_{0.3}TaO_3$.

For $x = 0.2$ and 0.3, the SAED investigations indicated them both to have the same supercell of perovskite, $a = b \approx \sqrt{2}a_{per}$ and $c \approx 2a_{per}$. This is clearly seen in the three SAED patterns of $Na_{0.8}Sr_{0.2}TaO_3$ in Fig. 5. They are viewed along [001], [100], and [210], corresponding to $\langle 100\rangle_{per}$, $\langle 110\rangle_{per}$, and $\langle 310\rangle_{per}$ in the ideal cubic perovskite structure, respectively. In each of the SAED patterns two reflections belonging to the basic perovskite sublattice are indexed according to the supercell. The same types of

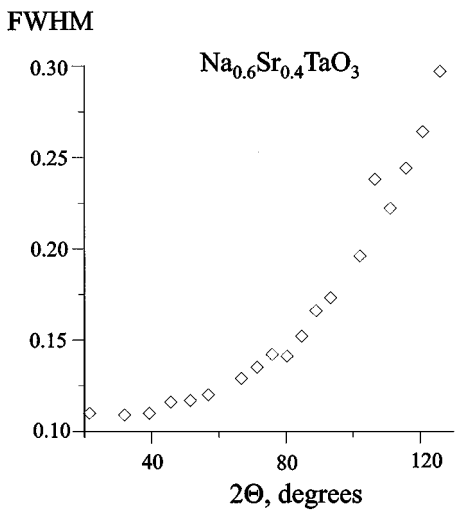

FIG. 4. Cubic symmetry is indicated by the monotonic increase with increasing Bragg angle, 2θ, of the FWHM of the XRD reflections for a sample with the nominal composition $Na_{0.6}Sr_{0.4}TaO_3$.

TABLE 2
Final Atomic Coordinates and Displacement Parameters for $Na_{1-x}Sr_xTaO_3$, $0 < x \leq 0.4$

Phase	Atom	x	y	z	B, Å^2
$Na_{0.6}Sr_{0.4}TaO_3$	Na/Sr	0.0	0.0	0.0	0.62(3)
	Ta	0.5	0.5	0.5	0.19(1)
	O	0.5	0.5	0.0	0.50(6)
$Na_{0.7}Sr_{0.3}TaO_3$	Na/Sr	0.0	0.0	0.0	1.6(6)
	Ta	0.5	0.5	0.5	0.8(2)
	O1	0.5	0.5	0.0	2 (1)
	O2	0.5	0.0	0.5	2 (1)
$Na_{0.8}Sr_{0.2}TaO_3$	Na/Sr	0.0	0.5	0.5	0.55(2)
	Ta	0.0	0.0	0.0	0.25(1)
	O1	0.0	0.0	0.5	0.71(6)
	O2	0.2841(7)	0.5–x	0.0	0.71(6)
$Na_{0.9}Sr_{0.1}TaO_3$	Na/Sr	0.002(2)	0.25	−0.015(2)	1.3(1)
	Ta	0.0	0.0	0.5	0.25(1)
	O1	−0.039(2)	0.25	0.448(3)	1.5
	O2	0.273(2)	−0.018(2)	0.273(2)	1.5

ED pattern were obtained for the $Na_{0.7}Sr_{0.3}TaO_3$ sample. Several of the SAED patterns showed that the superstructure reflections are affected by weak streaking along the c-axis indicating structural disorder. The $hk0$ pattern in Fig. 5a suggests reflections of the type $h00$, $h \neq 2n$, to be systematically absent, although some of them are present due to multiple scattering.

The presence of perovskite-type crystallites with tetragonal symmetry in the $x = 0.2$ and 0.3 samples is illustrated by the zero-order Laue zone (ZOLZ) and WP (whole-field pattern). CBED patterns recorded along [001], shown in Figs. 6 and 7. The symmetries of the ZOLZ and the WP (including higher-order Laue zones) patterns are all 4*mm*. This is in agreement with the two alternative diffraction groups 4*mm* and $4mm1_R$ (19, 20), which are consistent with the point groups 4*mm* and 4/*mmm* in the tetragonal system. However, the tetragonal symmetry was not observed all over the crystallites. Two possible reasons for this could be thickness variations or domains with lower symmetry, e.g., orthorhombic systems. We will discuss both possibilities below, starting with the assumption that the crystallites are single domains with tetragonal symmetry. In the ZOLZ pattern of $Na_{0.8}Sr_{0.2}TaO_3$, shown in Fig. 6a, dynamical absences (Gjönnes–Moodie (GM) lines) are seen in the 010 and 030 reflections. Equivalent GM lines have also been observed in ZOLZ patterns of $Na_{0.7}Sr_{0.3}TaO_3$. These lines support the systematic absences $0k0$, $k \neq 2n$ found in the $hk0$ SAED pattern shown in Fig. 5a above. The GM lines in combination with the observed 4*mm* symmetry of the diffraction pattern are indicative of two orthogonal glide planes, each parallel to a tetrad axis (4 and 4_2) and to the beam direction. Together with the point group, 4*mm* or 4/*mmm*, this gives eight possible space groups: *P*4*bm*, *P*4/*mbm*, *P*4$_2$*bc*, *P*4$_2$/*mbc*, *P*4$_2$*nm*, *P*4$_2$/*mnm*, *P*4*nc*, and *P*4/*mnc*. In the $0kl$ patterns of both $x = 0.2$ and 0.3 reflections of the type $k + l \neq 2n$ are systematically absent, as seen in Fig. 5b. In the hhl patterns (zone axis $[110] = \langle 001 \rangle_{per}$) the $l \neq 2n$ reflections are systematically absent or very weak (multiple scattering). These systematic absences limit the number of possible space groups to *P*4/*mnc* and *P*4*nc*. The space groups *P*4/*mnc* and *P*4*nc* are infrequent among perovskites of the ABO_3 type. However, ordered $A_2B'B''O_6$ perovskites (elpasolites) sometimes crystallize with one of these symmetries (21). In those cases the origin of the unit cell is chosen so that the B' and B'' atom positions both have the site symmetry 4.2, but with large and small octahedra. In the present compound, $Na_{1-x}Sr_xTaO_3$, it is not likely to find two types of TaO_6

TABLE 3
Selected Interatomic Distances and Angles (deg) in $Na_{1-x}Sr_xTaO_3$, $0 < x \leq 0.4$

Distance	$Na_{0.6}Sr_{0.4}TaO_3$	$Na_{0.7}Sr_{0.3}TaO_3$	$Na_{0.8}Sr_{0.2}TaO_3$	$Na_{0.9}Sr_{0.1}TaO_3$
Na/Sr–O1	2.802 (×12)	2.7913(1) (×4)	2.602(3) (×4)	2.57(2)
				2.56(2)
				2.98(2)
				3.01(2)
Na/Sr–O2		2.7887(1) (×8)	2.778 (×4)	2.49(2) (×2)
			2.979(3) (×4)	2.76(2) (×2)
				2.79(2) (×2)
				3.03(2) (×2)
Na/Sr–O mean	2.802	2.790	2.786	2.772
Ta–O1	1.981	1.9700(1) (×2)	1.973 (×2)	1.991(3) (×2)
Ta–O2		1.9738(1) (×4)	1.982(4) (×4)	1.97(1) (×4)
Ta–O mean	1.981	1.972	1.979	1.977
Ta–O1–Ta	180	180	180	166.7(7)
Ta–O2–Ta	180	180	164.5(2)	159.2(7)

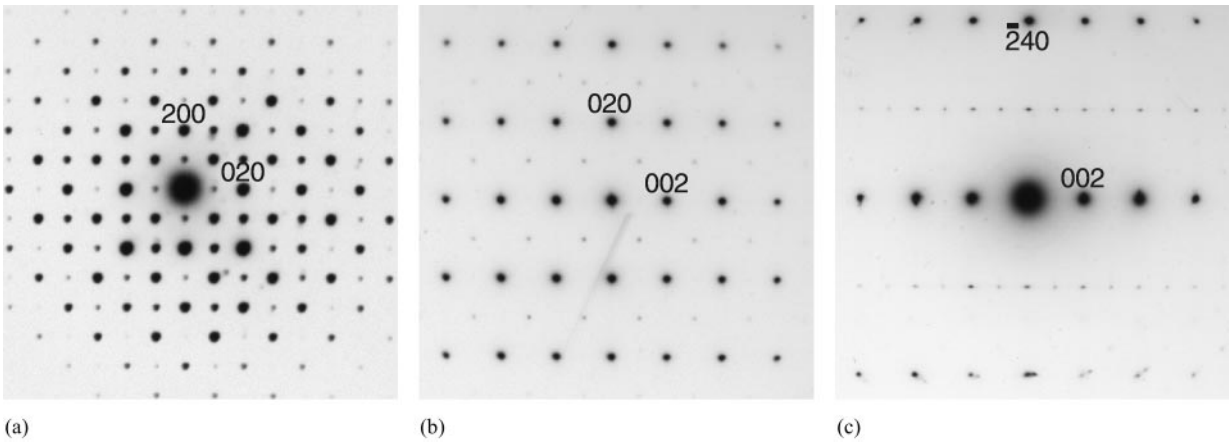

FIG. 5. SAED patterns of crystallites found in a sample with the nominal composition $Na_{0.7}Sr_{0.3}TaO_3$: (a) An $hk0$ ED pattern, zone axis $[001] = \langle 001 \rangle_{per}$. The reflections corresponding to $h00$, $h \neq 2n$, are present due to multiple scattering. (b) A $0kl$ ED pattern, zone axis $[100] = \langle 110 \rangle_{per}$. Reflections corresponding to $k + l \neq 2n$ are systematically absent. (c) An ED pattern viewed along zone axis $[210] = \langle 310 \rangle_{per}$. The superstructure reflections with $h + k \neq 2n$ are affected by weak streaking along the c-axis which indicates disorder.

octahedra with different Ta–O distances assuming that there is no charge ordering of the Ta^{4+} and Ta^{5+}. This strongly questions the obtained space groups especially as a neutron powder diffraction (NPD) data of the $Na_{0.8}Sr_{0.2}TaO_3$ sample did not exhibit reflections corresponding to $c \approx 2a_{per}$ (22). Considering this information an alternative interpretation of the experimental data is necessary. The observations of streaking along the c-axis among the superstructure reflections indicate the structure of the crystallites to be discontinuous. This could also explain why tetragonal symmetry was not observed all over the crystallites. One alternative explanation could therefore be that the crystallites consist of domains with tetragonal and orthorhombic symmetry, respectively. The tetragonal domains would then have the unit cell parameters $a = b \approx \sqrt{2}a_{per}$ and $c \approx a_{per}$ and space group $P4/mbm$ or $P4bm$, which are common among perovskites, while the areas with orthorhombic symmetry have the unit cell parameters $a = b \approx \sqrt{2}a_{per}$ and $c \approx 2a_{per}$. The space group is most probably $Pnma$ as it is found for $x = 0.1$ and has the same systematical absences as $P4/mnc$ and $P4nc$. The amount of the orthorhombic domains has to be small as no reflections

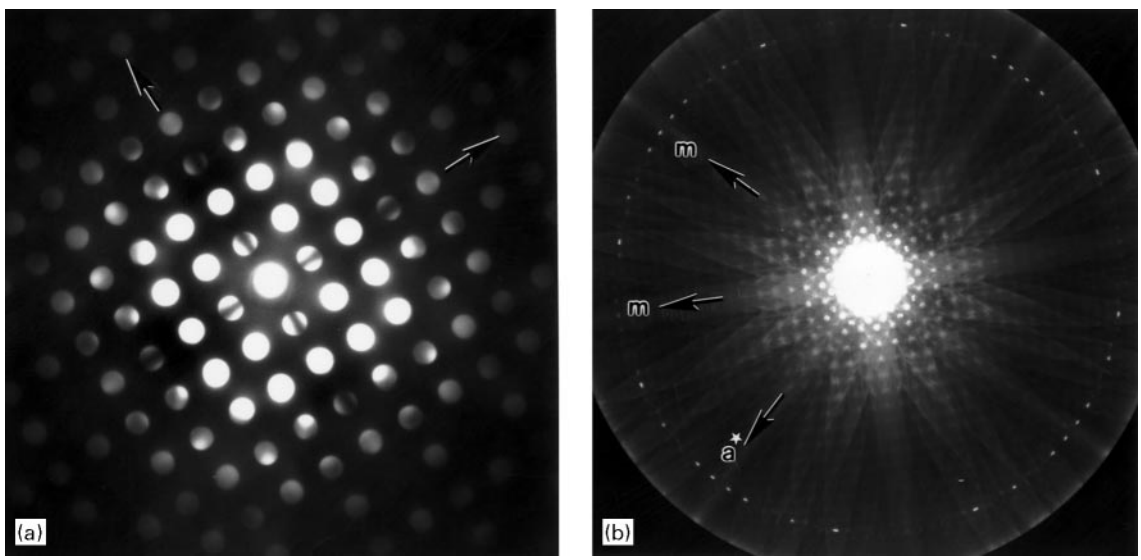

FIG. 6. (a) ZOLZ and (b) whole (WP) CBED patterns with $4mm$ symmetry of a crystallite in a sample with the nominal composition $Na_{0.8}Sr_{0.2}TaO_3$, viewed along $[001] = \langle 100 \rangle_{per}$.

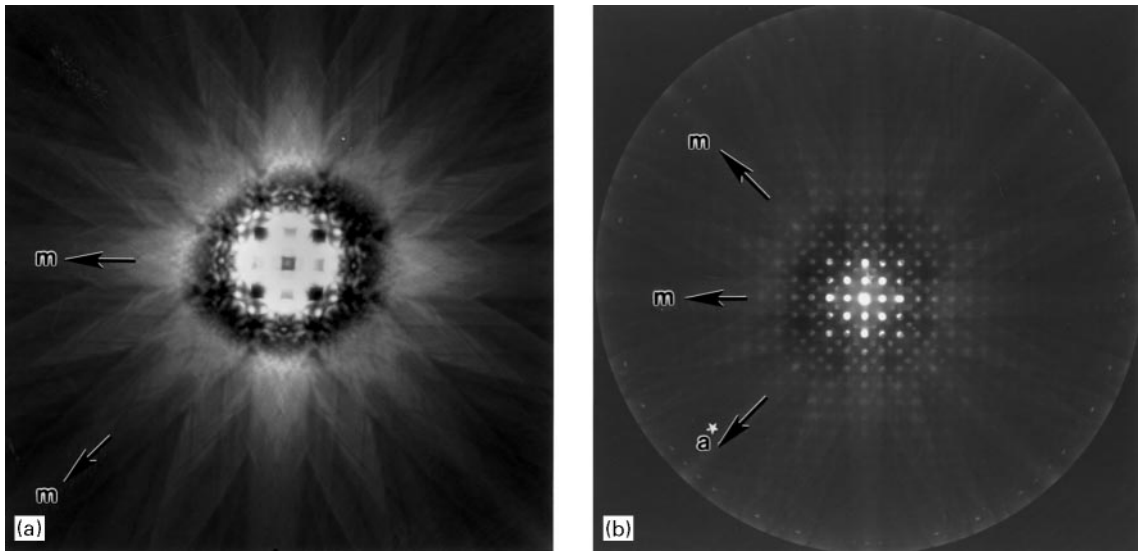

FIG. 7. (a) BF and (b) WP patterns of crystallites found in a sample with nominal composition $Na_{0.7}Sr_{0.3}TaO_3$, both with 4*mm* symmetry, viewed along $\langle 001 \rangle_{per}$.

indicating $c \approx 2a_{per}$ were found in the XRD nor in the NPD patterns and no splitting was observed in the low-temperature X-ray powder diffraction pattern. A more detailed structural study using neutron diffraction data is in progress.

For $x = 0.4$, the ED patterns indicated the simple cubic unit cell found in the XRD investigations to be correct. However, it should be mentioned that crystallites yielding weak superstructure reflections, similar to those of the $Na_{0.8}Sr_{0.2}TaO_3$ and $Na_{0.7}Sr_{0.3}TaO_3$ samples, were occasionally found. These crystallites probably had a slightly lower Sr content than $x = 0.4$.

Resistivity and Magnetic Measurements

The resistivity measurements revealed all samples to be nonmetallic conductors, see Fig. 8. The increase of resistance with decreasing temperature is less pronounced for the samples with higher strontium content, and their absolute resistivity values are lower; the $x = 0.1$ sample has $\approx 1.0\,\Omega$ at 300 K and the $x = 0.4$ sample $\approx 30\,\mu\Omega$ at 300 K.

Magnetic measurements were performed on the $x = 0.4$ sample and reveal a very weak diamagnetic behavior down to 20 K, changing to a slight paramagnetism at lower temperatures, see Fig. 9. The diamagnetic behavior is caused by the atomic-core contributions, while the increase of the susceptibility at low temperature can be explained either by the weak paramagnetism of Ta^{4+} or by the presence of paramagnetic admixtures. It should be mentioned that slightly reduced oxoniobates also show a very weak paramagnetism arising from Nb^{4+}. It is probably due to the strong spin–orbit coupling in Nb^{4+} (23), which should be even stronger for Ta^{4+}.

CONCLUSIONS

The XRD and ED studies both show that the symmetry of the crystal structure of $Na_{1-x}Sr_xTaO_3$ increases with the

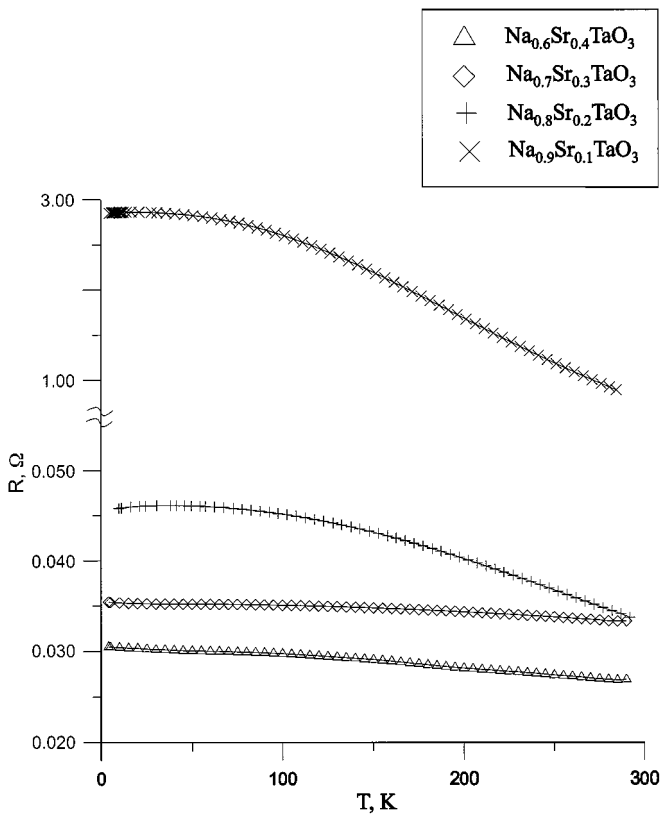

FIG. 8. Temperature dependence of the resistance of samples with nominal compositions $Na_{1-x}Sr_xTaO_3$ ($0 < x \leq 0.4$).

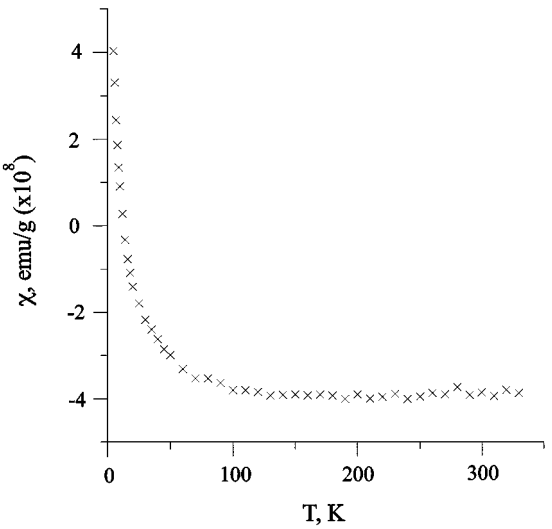

FIG. 9. Temperature dependence of the magnetic susceptibility of a sample with nominal composition $Na_{0.4}Sr_{0.6}TaO_3$.

Sr content. The distorted structure of $NaTaO_3$ is in agreement with the value $t = 0.967$ of the tolerance factor ($t = (R_A + R_O)/[2^{1/2}(R_M + R_O)]$, $r(Na^+) = 1.39$ Å, $r(Ta^{5+}) = 0.64$ Å, $r(O^{2-}) = 1.40$ Å (24)). This tolerance factor was first introduced by Goldschmidt, and it describes how well the structure fits a cubic close packing of A and O atoms with M in octahedral cavities (25). A perfect fit is obtained for $t = 1.00$. The tolerance factor of the hypothetical $SrTaO_3$, $t = 0.965$, ($r(Sr^{2+}) = 1.44$ Å, $r(Ta^{4+}) = 0.68$ Å) is very similar to that of $NaTaO_3$. The structural changes are more likely to be caused by the population of π-bonding M–O orbitals stabilizing an M–O–M bond angle of 180° (11, 12). This is also observed in the average structures obtained from Rietveld refinements, using XRD data. The differences between axial and equatorial Ta–O distances within the TaO_6 octahedra increase from 0.004 Å for $Na_{0.7}Sr_{0.3}TaO_3$ (calculated from the unit cell parameters), to 0.02 Å for $Na_{0.9}Sr_{0.1}TaO_3$, see Table 3. Moreover, in the structure of $Na_{0.8}Sr_{0.2}TaO_3$, refined using XRD data, there is an additional rotation of the TaO_6 octahedra around [001]. The Ta–O1–Ta angle 164.5(2)°, deviates from the ideal 180° found for Ta–O2–Ta (see Table 3.) The structure of $Na_{0.9}Sr_{0.1}TaO_3$ ($GdFeO_3$ type) corresponds to a 3-tilt system $a^-c^+a^-$, in Glazer notation (17). In this structure both the Ta–O1–Ta and Ta–O2–Ta angles are different from the ideal 180° value. A more detailed study of the structural changes in the $Na_{1-x}Sr_xTaO_3$ system, using neutron diffraction, is in progress.

The homogeneity region of $Na_{1-x}Sr_xTaO_3$ ($0 \le x \le 0.4$) is narrower than that reported for $Na_{1-x}Sr_xNbO_3$ ($0 \le x \le 0.6$) (26). This is not surprising, considering that tantalum has a lower preference than niobium for the formal oxidation state +4 in oxide compounds. Moreover, during the synthesis the samples lose sodium, which leads to the formation of vacancies at the A sites and consequently to an increase in the formal oxidation state of tantalum. The lowest oxidation state of tantalum that can be achieved in $Na_{1-x}Sr_xTaO_3$ is therefore +4.7, found for a sample with the nominal composition $Na_{0.6}Sr_{0.4}TaO_3$.

ACKNOWLEDGMENTS

The authors thank E. Bruecher for the magnetic measurements and G. Siegle for the resistivity measurements. G.S. thanks the Swedish Natural Science Council for financial support. S.Ya.I. is also grateful to the Max-Planck-Gesellschaft for financial support.

REFERENCES

1. D. Ridgley and R. J. Ward, *J. Am. Chem. Soc.* **77,** 6132 (1955).
2. B. Hessen, S. A. Sunshine, T. Siegrist, and R. Jimenez, *Mater Res. Bull.* **26,** 85 (1991).
3. B. Hessen, S. A. Sunshine, T. Siegrist, A. T. Fiory, and J. V. Waszczak, *Chem. Mater.* **3,** 528 (1991).
4. H. Fukuoka, T. Isami, and S. Yamanaka, *Chem. Lett.* **8,** 703 (1997).
5. J. Köhler, G. Svensson, and A. Simon, *Angew. Chem.* **104,** 1463 (1992); *Angew. Chem., Int. Ed. Engl.* **31,** 1437 (1992).
6. T. Siegrist, R. J. Cava, and J. J. Krajewski, *Mater. Res. Bull.* **32,** 881 (1997).
7. C. R. Feger and R. P. Ziebarth, *Chem. Mater.* **7,** 373 (1995).
8. K.Toda, M. Takahashi, T. Teranishi, Z.-G. Ye, M. Sato, and Y. Hinatsu, *J. Mater. Chem.* **9,** 799 (1999).
9. B. Harbrecht and A. Ritter, *Z. Anorg. Allg. Chem.* **625,** 178 (1999).
10. B. Harbrecht, V. Wagner, and A. Ritter, *Z. Anorg. Allg. Chem.* **624,** 457 (1998).
11. J. B. Goodenough, *Prog. Sol. State Chem.* **5,** 145 (1971).
12. P. M. Woodward, *Acta Crystallogr. B* **53,** 44 (1997).
13. R. A. Wheeler, M. H. Whangbo, T. Hughbanks, R. Hoffmann, J. K. Burdett, and T. A. Albright, *J. Am. Chem. Soc.* **108,** 2222 (1986).
14. F. Izumi, *Rikagu J.* **6,** 10 (1989).
15. R. Kilaas, MacTempas: Program for simulating High Resolution TEM Images and Diffraction Patterns, Total Resolution, Berkeley, CA, 1994.
16. M. Ishizawa, *Acta. Crystallogr. B* **32,** 2564 (1976).
17. A. M. Glazer, *Acta Crystallogr. A* **31,** 756 (1975).
18. M. Ahtee and C. N. W. Darlington, *Acta Crystallogr. B* **36,** 1007 (1980).
19. D. B. Williams and C. B. Carter, "Transmission Electron Microscopy II." Plenum, New York, 1996.
20. B. F. Buxton, J. A. Eades, J. W. Steeds, and G. M. Rackham, *Philos. Trans. R. Soc.* **281,** 181 (1976).
21. I. N. Flerov, M. V. Gorev, K. S. Aleksandrov, A. Tressaud, J. Grannec, and M. Couzi, *Mater. Sci. Eng.* **24,** 81 (1998).
22. S. Ya. Istomin and G. Svensson, private communication.
23. S. Ya. Istomin, O. G. Dyachenko, E. V. Antipov, G. Svensson, and B. Lundqvist, *Mater. Res. Bull.* **33,** 1251 (1998).
24. R. D. Shannon and C. T. Prewitt, *Acta Crystallogr. B* **35,** 745 (1969).
25. V. M. Goldschmidt, *Naturwissenschaften* **14,** 477 (1926).
26. B. Ellis, J.-P. Doumerc, M. Pouchard, and P. Hagenmuller, *Mater. Res. Bull.* **19,** 1237 (1984).